ACS Catalysis

RESEARCH ARTICLE

pubs.acs.org/acscatalysis

Ab Initio Study on a Novel Photocatalyst: Functionalized Graphitic Carbon Nitride Nanotube

Hui Pan,*[,†] Yong-Wei Zhang,[†] Vivek B. Shenoy,[‡] and Huajian Gao[‡]

[†]Institute of High Performance Computing, 1 Fusionopolis Way, Singapore 138632, Singapore

[‡]Division of Engineering, Brown University, 610 Barus & Holley, 182 Hope Street, Providence, Rhode Island 02912, United States

Supporting Information

ABSTRACT: A novel nanomaterial, graphitic carbon nitride nanotube, was designed and studied for its application to photocatalyst by first-principles calculations. This nanomaterial is semiconducting with size-dependent bandgap and stable in an extreme environment. Most interestingly, its electronic structure with adjustable bandgap can be easily modified by functionalizing with metal atoms. The calculated electronic and optical properties of functionalized nanotube evidence the narrowed bandgap and optical gap, and enhanced mobility, satisfying basic prerequisites as a new class of high efficiency photocatalysts for water splitting and other avenues of solar energy utilization. The functionalized nanotubes may enable efficient solar energy conversion in a variety of industrial and environmental applications.

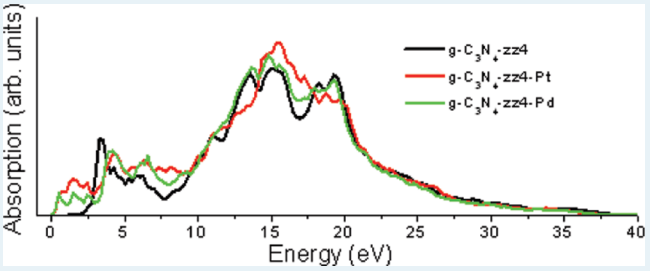

KEYWORDS: graphitic carbon nitride nanotube, functionalization, bandgap and optical gap, visible-light absorption, photocatalyst, first-principles calculation

I. INTRODUCTION

The search for sustainable alternative energy sources has attracted increasing attention because of the limited supply of the old forms of depletable energy (coal, oil, nuclear) and their detrimental effects on the global climate. Solar energy is considered to be the most important candidate because it is abundant, clean, and renewable. A variety of technologies have been developed to take advantage of solar energy, such as photovoltaic cell (PV) and photoelectrochemical cell (PEC). The PV can directly convert the solar energy to electrical energy. The PEC splits water into hydrogen and oxygen, so as to convert the solar energy into chemical energy. Because of the versatile applications of hydrogen and oxygen gases, the PEC has attracted substantial attention since the discovery of water splitting property of TiO_2 electrodes under ultraviolet (UV) illumination.[1] However, the UV irradiation only accounts for ~5% of the solar spectrum and, as a consequence, the efficiency of solar energy conversion by this process is limited because of its wide bandgap (~3.0 eV). To enhance the light-absorption efficiency, considerable effort has been conducted to fine-tune its bandgap for the visible-light absorption, such as chemical functionalization and defect engineering,[2−8] but only limited success has been achieved to date. Design of new photocatalysts is thus a critical step to solar energy harvesting. The development of efficient photocatalysts should satisfy the following: (1) an optimal band structure for maximal utilization of solar energy,[2,7,9,10] (2) efficient photoinduced electron−hole separation and high carrier mobility,[11] (3) large contacting surface area with the electrolyte,[3] and (4) high stability in extreme environments.[12] On the basis of these principles, many new photocatalysts using transition-metal oxides as the main component have been proposed and tested.[13] However, the low carrier mobility and high recombination rate in oxides induced by the localized band edge limit the conversion efficiency. Recently, a solid solution of gallium nitride and zinc oxide ($Ga_{1-x}Zn_xN_{1-x}O_x$) was reported to be stable and capable of water splitting under visible light because of the narrowing of the bandgap of GaN.[14,15] Also, a metal-free compound, graphitic carbon nitride (g-C_3N_4), was reported to be suitable for water splitting under visible light illumination.[16] The delocalized s/p states of these materials may shed light on the enhancement of carrier mobility. In the present study, g-C_3N_4 nanotube was designed for possible applications in solar energy conversion by first-principles calculation. We found that the conversion efficiency can be improved by functionalizing the nanotubes with metal atoms because of the narrowing of bandgap, enhancement of visible-light absorption, and improvement of mobility compared with the material without doping.

II. METHODS

The first-principles calculation was carried out based on the density function theory (DFT)[17] and the generalized gradient approximation (GGA)[18] as incorporated in the Vienna ab initio

Received: October 12, 2010
Revised: December 15, 2010
Published: January 18, 2011

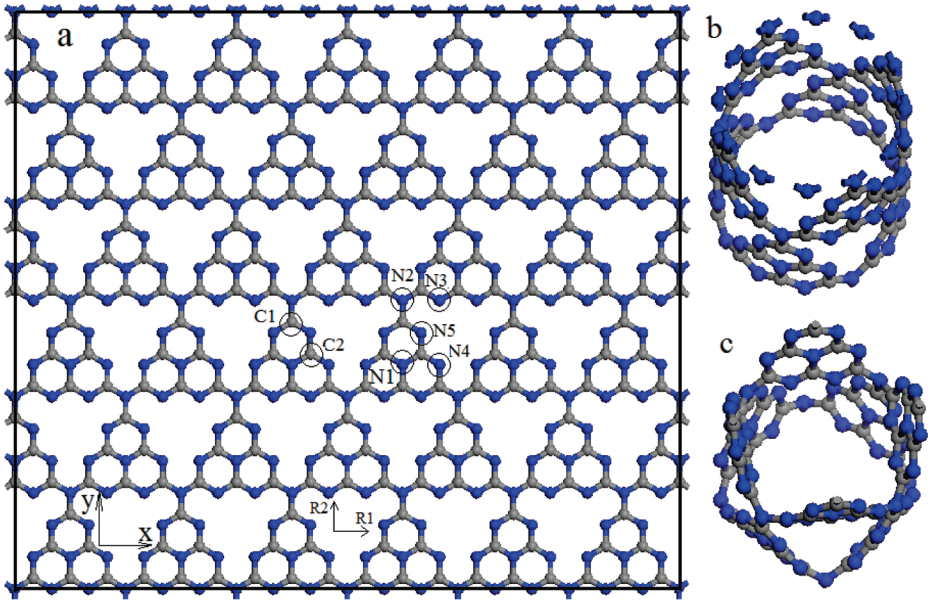

Figure 1. Atomic configurations of g-C_3N_4. (a) monolayer, and nanotube (b) before and (c) after geometry optimization. The C and N atoms are indicated by gray and blue spheres, respectively. The wrapping vector of the nanotube is along the *x* axis (R1) shown in (a).

simulation package (VASP).[19] The Monkhorst and Pack scheme of k point sampling was used for integration over the first Brillouin zone.[20] The most stable structure of carbon nitride is the graphitic phase, g-C_3N_4, which is a heptazine-based form (Figure 1a).[21] The geometries of g-C_3N_4 with the AB structure and one g-C_3N_4 monolayer were first optimized to get the lattice constants. For the monolayer, a vacuum space with 12 Å was used to minimize the interlayer's interaction. A 5 × 1 × 1 grid for k-point sampling and an energy cutoff of 400 eV were used for the bulk and monolayer. Our g-C_3N_4 nanotube is constructed by curling up one monolayer into a cylinder along the axial (x) direction (Figure 1b). A 1 × 1 × 3 grid for k-point sampling and an energy cutoff of 400 eV were consistently used in our calculations on the g-C_3N_4 nanotubes. Good convergence was obtained using these parameters, and the total energy was converged to 2.0 × 10^{-5} eV/atom. A large supercell dimension with a wall−wall distance of 10 Å in the plane perpendicular to the tube axis was used to avoid interaction between the nanotube and its images in neighboring cells. The periodic unit in the axial direction is 12.35 Å.

To modify the electronic structure of the g-C_3N_4 nanotubes for their application in solar energy conversion, functionalization of the nanotube was investigated by doping the nanotube with metal elements. The functionalization energy is estimated from

$$E_f = (E_{tot}(tube + doping) - E_{tot}(tube) - n\mu_{doping})/n$$

where $E_{tot}(tube+doping)$ and $E_{tot}(tube)$ are the total energies of the g-C_3N_4 with and without doping, respectively; μ_{doping} is the chemical potential (the energy required to remove an atom from its bulk) of the metal element, and n is the number of the metal atoms.[22] The spin polarization of the transition metal atom is considered in the functionalized nanotubes.

III. RESULTS AND DISCUSSION

After geometry optimization, the calculated distance between two nitride pores is 7.133 Å, consistent with the experimental value (7.13 Å), and the calculated interlayer distance of the AB g-C_3N_4 bulk is 3.543 Å, larger than the experimental value (3.26 Å).[16] The in-plane repeated period of the g-C_3N_4 monolayer in the x direction is 7.129 Å, slightly smaller than that of its corresponding bulk. The band structure and partial density of states (PDOS) (see Supporting Information, S-1) show that the valence top states are strongly localized and the mobility is lower, suggesting the low photocatalytic ability of g-C_3N_4 in water. To improve the efficiency, a new nanostructure, g-C_3N_4 nanotube, was constructed and investigated for its applications in PV and PEC.

The g-C_3N_4 nanotube is obtained by rolling up the g-C_3N_4 monolayer. There can be more than one type of g-C_3N_4 nanotubes, depending on how the g-C_3N_4 monolayer is rolled up. Here, we only consider the g-C_3N_4 nanotube constructed from rolling up the monolayer along the x direction (R1 in Figure 1a), which is defined as a zigzag tube, adopting a similar terminology used in other nanotubes.[23] Four zigzag g-C_3N_4 nanotubes (n, 0) with n = 3−6 were investigated in our study, labeled as g-C_3N_4-zzn (n = 3−6). As an indication of structural stability, the total energy of the optimized g-C_3N_4 nanotube was calculated and compared with those of graphitic and monolayer C_3N_4 (Figure 2). Interestingly, the total energy per C_3N_4 unit of g-C_3N_4-zzn (n > 3), which decreases rapidly with increasing diameter, drops below those of graphitic and monolayer C_3N_4 beyond a critical size, indicating that the nanotube can be more stable and may be produced experimentally. We can see that the heptazine structures in the optimized geometry of g-C_3N_4-zz4 remain almost as flat as those in the monolayer after the optimization (Figure 1c). A large curvature with the up C−N−C angle reduced to 106° is observed at the heptazine-heptazine N connection, consistent with the literature.[24] However, the lattice distortion both in the heptazine and at the connection is less than 0.5%.

The calculated band structures of the g-C_3N_4 nanotubes (Figure 3) show unique properties which are different from that of the monolayer (See Supporting Information, S-1). The bandgap of the g-C_3N_4 nanotube increases with increasing size (n) and should be converged at larger diameter, which is opposite

dx.doi.org/10.1021/cs100045u |*ACS Catal.* 2011, 1, 99–104

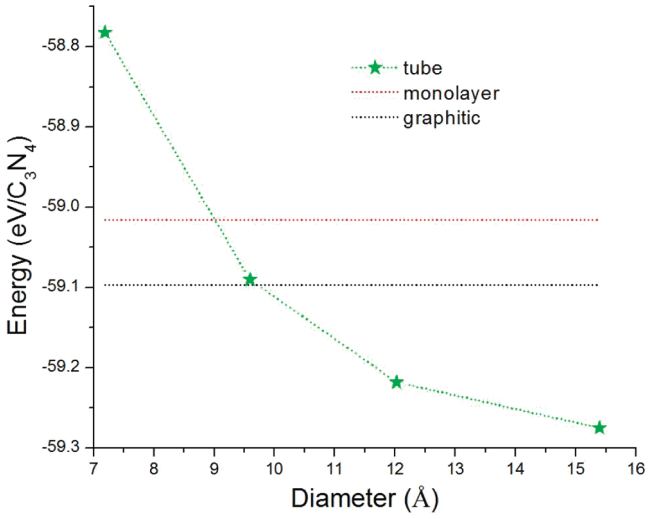

Figure 2. Total energy per C_3N_4 unit of the g-C_3N_4 nanotubes as a function of the tube diameter. For comparison, the total energies per C_3N_4 unit of the g-C_3N_4 monolayer and bulk are presented.

to the trend of single-walled carbon nanotubes,[25] but similar to that of other compound nanotubes.[26] The g-C_3N_4-zz3 is a semiconductor with a direct bandgap of 1.35 eV. Both of its valence band top (VBT) and conduction band bottom (CBB) are at Γ-point (Figure 3a). Contrary to the localized VBT in the g-C_3N_4 monolayer, the valence top states of g-C_3N_4-zz3 are delocalized as indicated by the dispersion of the VBT in the band structure (Figure 3a). The band structure changes as the nanotube size increases. The g-C_3N_4-zz4 has a direct bandgap of 1.59 eV (Figure 3b). However, the dispersion of the VBT of g-C_3N_4-zz4 is not as apparent as that of g-C_3N_4-zz3, indicating the limited delocalization of the valence top states. The localization becomes more and more apparent with the increase of nanotube diameter. The g-C_3N_4-zz5 and g-C_3N_4-zz6 are indirect semiconductors with the VBT at Z-point and the CBB at Γ-point (Figures 3c and 3d), and have a bandgap of 1.68 and 1.71 eV, respectively. The topmost valence bands of g-C_3N_4-zz5 and g-C_3N_4-zz6 are dispersionless, indicating that they are strongly localized states. The bandgaps of the nanotubes are larger than that of the monolayer (1.127 eV, Supporting Information, S-1) because of the distortion of structures in the nanotubes (Figure 1c) and different origins for the band edge states as discussed below.

The partial density of states (PDOS) analysis reveals that the origins of VBT and CBB in g-C_3N_4 nanotubes are different from those in the monolayer. As shown in Figure 4, the valence top states of g-C_3N_4-zz4 are dominated by the p electrons of the N center atoms (N1 in Figure 1a). Its conduction bottom states are dominated by the p electrons of nitrogen atoms at the edge (N3 in Figure 1a) and carbon atoms at the connection (C1 in Figure 1a) and edge (C2 in Figure 1a), indicating that the carriers are localized in the tri-s-triazine unit. For monolayer, its VBT is dominated by the p electrons of the nitrogen atoms at the edge (N3) (Supporting Information, S-1). The energy levels induced by the dangling states of N3 results in the smaller bandgap of the monolayer (Supporting Information, S-1). Although the carrier mobility in the nanotubes is as low as that in the monolayer (Supporting Information, S-1), the mobility may be enhanced as indicated by the VBT dispersion because of the reduced effective mass (Figure 3). The energy conversion efficiency may be improved by designing the nanotubes with different diameters. However, the localized states and enlarged bandgap in the nanotubes with larger diameters may reduce the efficiency because of lower carrier mobility and reduced visible-light absorption. The dispersion of VBT is related to the effective mass and mobility of a hole in semiconductors. For p-type semiconductor, the majority carriers are holes and minority carriers are electrons, whereas the situation is reversed for n-type semiconductor. For a photocatalyst, an electron−hole pair is created by the photon illumination: electrons transport to the cathode, resulting in hydrogen gas; holes transport to the anode, leading to oxygen gas. Therefore, both electron mobility and hole mobility are important to the efficiency.

Functionalization of single-walled carbon nanotubes has been widely used to modify their electronic, chemical, optical, and mechanical properties.[27−29] This suggests that the conversion efficiency of g-C_3N_4 nanotubes may be enhanced by improving carrier mobility and electron−hole separation, and narrowing the bandgap through functionalization. In our calculations, to modify the electronic properties of g-C_3N_4 nanotube, two metal elements (also good catalysts for hydrogen generation), Pd and Pt, were used to functionalize the g-C_3N_4-zz4 by putting the metal elements at the center of triangular pores, one atom per pore, initially. The calculated functionalization energies are 1.92, and 3.62 eV per atom for Pd and Pt, respectively, suggesting that the functionalization of Pd is easier than that of Pt because of the relatively lower functionalization energy.

By comparing the band structures of nanotubes with and without Pd (Figures 3b and 5a), we can see that the Fermi level was shifted into the conduction band by functionalizing the tube with Pd, indicating the Pd-functionalized nanotube is a heavily doped n-type semiconductor or becomes metallic (Figure 5a). However, the Pt-functionalized g-C_3N_4-zz4 (g-C_3N_4-zz4-Pt) remains intrinsic (Figure 5b). The Fermi level shifting strongly depends on doping concentration and elements, and the host material itself. Importantly, the bandgaps of the functionalized nanotubes are smaller than that of the nanotube without functionalization. The narrowing of the bandgap suggests the enhanced absorption and utilization of sunlight. The carrier mobility is also improved by the functionalization although the improvement depends on the functionalizing metals. Compared with Pd-functionalized nanotube, the g-C_3N_4-zz4−Pt has more delocalized valence top states indicated by the wide dispersion of VBT (Figure 5b). The enhancement of mobility and the narrowing of bandgap lead to the improvement of conversion efficiency in Pt-functionalized nanotubes. We also studied the metal cluster (four metal atoms, M4) doped nanotube. We found that the cluster distorts the nanotube and itself was also distorted by forming bonds with C, N, or both in the nanotube. Therefore, the metal-functionalized nanotubes were not considered as co-catalyst, but a new catalyst, graphitic metal−carbon nitride nanotube. The smooth structures of the nanotubes doped with one atom per pore indicated that they are single-phase catalysts (Figures 6a and 7a), which will be discussed below in detail.

To understand the origins of the enhancement, we investigated the geometrical structures and PDOSs of the functionalized nanotubes. The optimized g-C_3N_4-zz4-Pt (Figure 6a) looks more like a cylinder than the g-C_3N_4-zz4 without functionalization (Figure 1c). The curvature in the g-C_3N_4-zz4-Pt is uniform, and the heptazine structure is not a plane. Geometrically, one Pt atom has two bonds with a length of 2.15 Å, chemically connecting the edge nitrogen atoms (N5 in Figure 1a), and the g-C_3N_4-zz4-Pt has a smooth curvature (Figure 6a). These

dx.doi.org/10.1021/cs100045u |ACS Catal. 2011, 1, 99–104

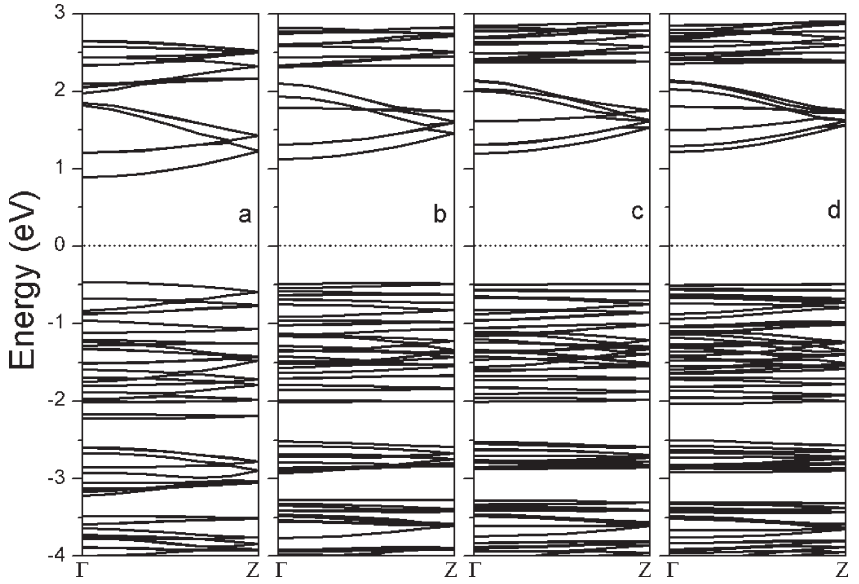

Figure 3. Calculated band structures. (a) g-C_3N_4-zz3, (b) g-C_3N_4-zz4, (c) g-C_3N_4-zz5, and (d) g-C_3N_4-zz6. The Fermi level is shifted to 0 eV (dotted line).

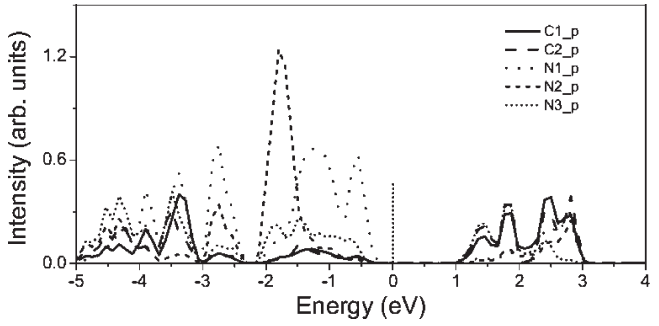

Figure 4. Calculated PDOS of the g-C_3N_4-zz4. The Fermi level is shifted to 0 eV (dotted line).

chemical bonds connect the heptazines together and provide more paths for the carrier transport besides the nitrogen connection. The delocalized valence top and conduction bottom states, leading to the improvement of mobility, are mainly contributed by the Pt-d electrons and p electrons of carbon atoms and edge nitrogen atoms bonded with Pt atoms (N5 in Figure 1a) (Figure 6b). Importantly, the g-C_3N_4-zz4-Pt is a direct semiconductor with a gap of 0.32 eV (Figure 5b), which results in efficient absorption of solar energy. It is predicted that Pt-functionalization can significantly enhance the solar energy conversion efficiency of the g-C_3N_4 nanotubes because of the narrowed bandgap and enhanced mobility. The valence top states are more localized for g-C_3N_4-zz4-Pd (Figure 5a), possibly because of the similar geometrical structures between g-C_3N_4-zz4-Pd (Figure 7a) and g-C_3N_4-zz4 (Figure 1c). The PDOS analysis demonstrates that the VBT is dominated by Pd-d electrons and has partial contribution from p electrons of carbon atoms and the edge nitrogen atoms (N4 in Figure 1a), and CBB are dominated by the Pd-d electrons (Figure 7b). Although the bandgap of the Pd-functionalized nanotubes is larger than that of g-C_3N_4-zz4-Pt, it (0.62 eV) is less than that of g-C_3N_4-zz4 (1.47 eV), which leads to the enhancement of sunlight adsorption and contributes to the efficiency improvement.

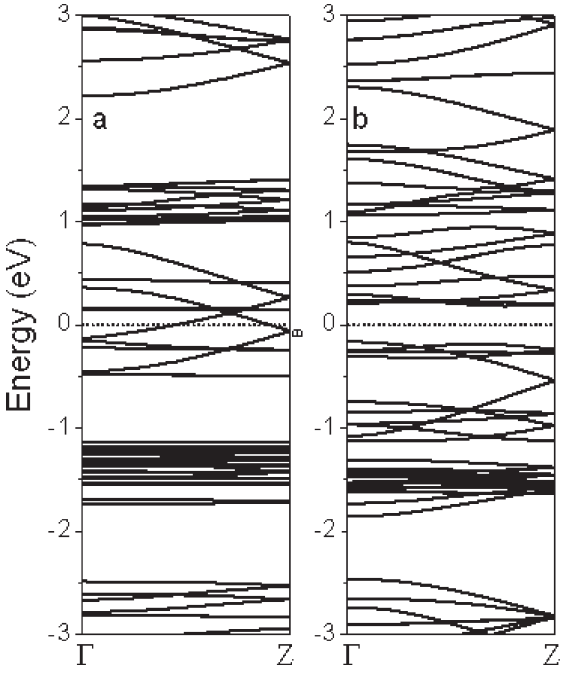

Figure 5. Calculated band structures: (a) g-C_3N_4-zz4-Pd, and (b) g-C_3N_4-zz4-Pt. The Fermi level is shifted to 0 eV (dotted line).

To further confirm the improvement of optical absorption in visible light for the functionalized nanotubes, we calculated the loss function which is a direct probe of the collective excitation of the system under consideration. The imaginary part of the dielectric constant was calculated from

$$\varepsilon_2(q \rightarrow O_{\hat{u}}, \hbar\omega) = \frac{2e^2\pi}{\Omega}\varepsilon_0 \sum_{k,v,c} |\langle \Psi_k^c | \hat{u}\cdot r | \Psi_k^v \rangle|^2 \delta(E_k^c - E_k^v - E)$$

where $\hat{u}$ is the vector defining the polarization of the incident electric field. This expression is similar to the Fermi's Golden rule

dx.doi.org/10.1021/cs100045u |ACS Catal. 2011, 1, 99–104

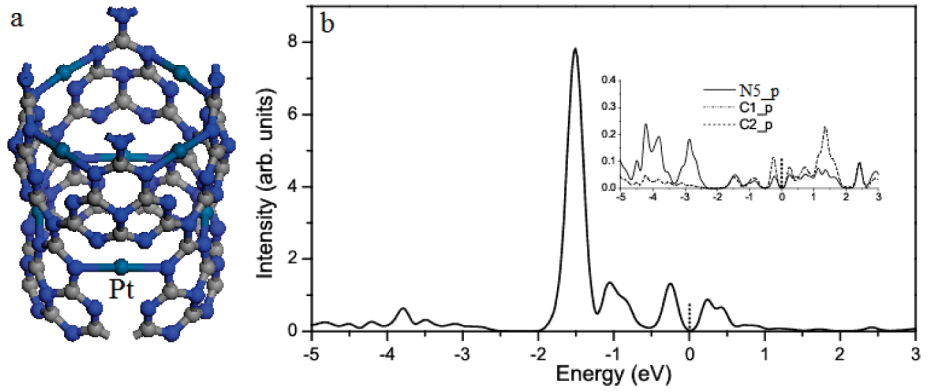

Figure 6. Optimized geometry (a) and the calculated PDOS of Pt-d electrons (b) of Pt-functionalized g-C_3N_4-zz4. The inset in (b) shows the PDOSs of C and N p electrons as indicated in Figure 1. The Fermi level is shifted to 0 eV (dotted line).

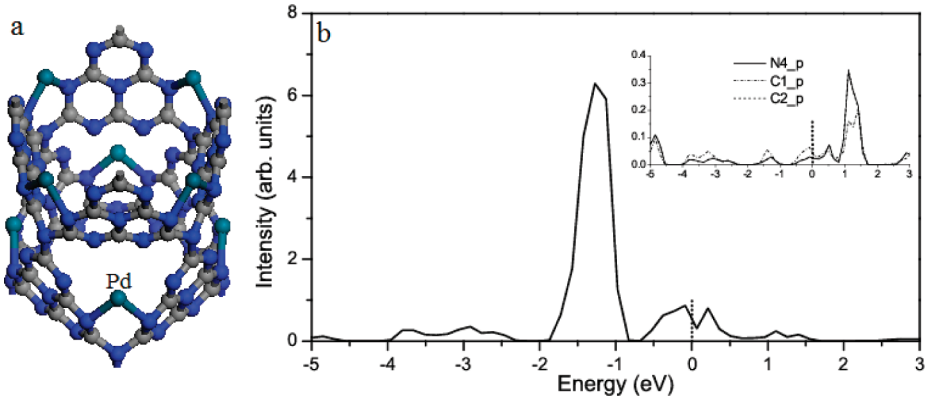

Figure 7. Optimized geometry of Pd-functionalized g-C_3N_4-zz4 (a) and calculated PDOS of Pd-d electrons (b) of Pd-functionalized g-C_3N_4-zz4. The inset in (b) shows the PDOSs of C and N p electrons as indicated in Figure 1. The Fermi level is shifted to 0 eV (dotted line).

for time dependent perturbations, and $\varepsilon_2(\omega)$can be thought of as detailing the real transitions between occupied and unoccupied electronic states. The real part, $\varepsilon_1(\omega)$, is obtained by the Kramers−Kronig relation. The loss function is calculated using $\mathrm{Im}(-1/\varepsilon(\omega))$ at zero momentum transfer from the macroscopic dielectric function $\varepsilon(\omega)$ $(\varepsilon(\omega) = \varepsilon_1(\omega) + i\varepsilon_2(\omega))$ for a periodic system. The calculated loss functions of g-C_3N_4-zz4 with and without functionalization show several peaks in the low energy range, which are related to the 1D subbands with divergent density of states (Figure 8). The pronounced peak in the loss function of g-C3N4-zz4 is at 3.3 eV, which is the optical gap and related to the interband excitation. The optical gaps for the functionalized nantubes are 0.71 and 0.5 eV for g-C_3N_4-zz4-Pt and g-C_3N_4-zz4-Pd, respectively. Clearly, the optical gap of the nanotube is narrowed after the functionalization, resulting in the improvement of optical absorption in the visible light. The absorption spectra of the nanotubes further confirmed the enhancement of light absorption in the lower-energy range (<3.2 eV) after functionalization (Figure 9). The g-C_3N_4-zz4 shows very weak visible-light absorption. Although the optical gap of g-C_3N_4-zz4-Pt is slightly larger than that of g-C_3N_4-zz4-Pd, the visible-light absorption of g-C_3N_4-zz4-Pt is better than that of g-C_3N_4-zz4-Pd, as indicated by the large area of the absorption spectrum of g-C_3N_4-zz4-Pt in the visible-light range (Figure 9). The minimal photo energy to excite electrons from the valence band to the conduction band is reduced because of the narrowed bangdap in the Pt-functionalized nanotube (Figure 5b), resulting in the enhancement of visible-light absorption (Figure 9). The bandgap of

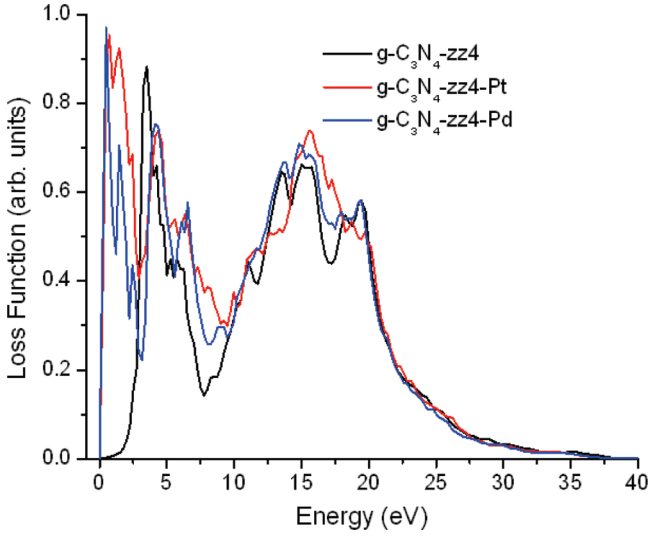

Figure 8. Calculated loss functions of g-C_3N_4-zz4 with and without functionalization.

Pt-functionalized nanotube (0.32 eV) is less than that of Pd-functionalized nanotube (Figure 5). And the valence top and conduction bottom states in Pt-doped nanotube are more delocalized than those in Pd-doped nanotube (Figure 5), resulting high carrier mobility in Pt-doped nanotube. All of these advantages lead to the

dx.doi.org/10.1021/cs100045u |*ACS Catal.* 2011, 1, 99–104

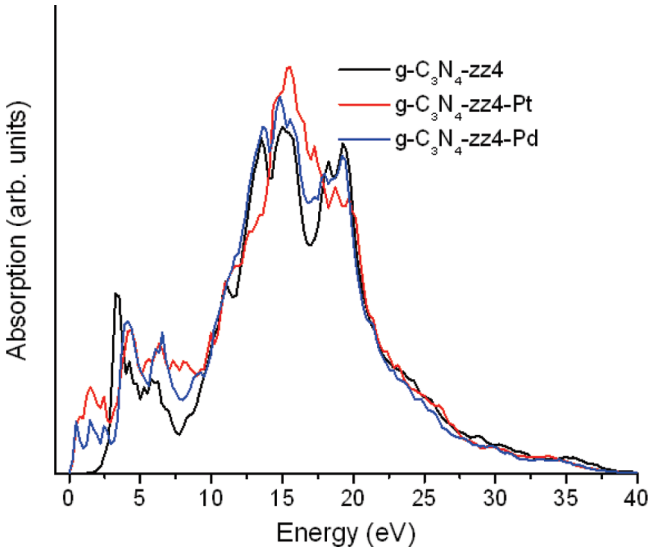

Figure 9. Calculated absorption spectra of g-C_3N_4-zz4 with and without functionalization.

better visible-light absorption. Although the optical gap of Pd-doped nanotube (0.5 eV) is less than that of Pt-doped one (0.71 eV), the smaller optical gap is attributed to the near band excitation, but not the interband transition of electrons because the Pd-doped nanotube is an n-type semiconductor, and the calculated optical gap is always larger than the calculated bandgap for an intrinsic semiconductor. The calculations of the metal-functionalized g-C_3N_4 nanotubes reveal that their electronic and optical properties, such as bandgap and optical gap, can easily be modified by functionalization. The conversion efficiency can be maximally improved by optimally functionalizing these nanotubes.

IV. CONCLUSIONS

In summary, novel g-C_3N_4-based nanotubes are proposed and designed based on the first-principles calculations for their application in solar energy conversion. Our calculation revealed that the nanotubes can efficiently utilize sunlight because their bandgaps are size-dependent. We found that the electronic and optical properties of the nanotubes can be easily adjusted by functionalization with metal atoms. The metal-functionalized nanotubes, as a new catalyst (graphitic metal−carbon nitride nanotube), with enhanced mobility, and narrowed bandgap and optical gap, enable the enhanced absorption and photoactivity in the visible-light region and may find applications in hydrogen generation and environmental cleanup. Although the GGA method always underestimates the bandgap of materials, the trend of the changes is correct and the conclusion is not affected. Additionally, the metals and metal nitrides in the functionalized nanotubes are corrosion-resistant, and may be used in extreme environments. It is also expected that the nanotubes with or without functionalization may also impact related application areas demanding high surface area and surface activity, such as hydrogen storage.[30]

■ ASSOCIATED CONTENT

Supporting Information. The electronic structures of g-C_3N_4 monolayer are shown in S1. This material is available free of charge via the Internet at http://pubs.acs.org.

■ AUTHOR INFORMATION

Corresponding Author

*E-mail: panh@ihpc.a-star.edu.sg. Phone: 65-64191425. Fax: 65-64674350.

■ ACKNOWLEDGMENT

This work has been supported by the A*Star Visiting Investigator Program "Size Effects in Small Scale Materials" hosted at the Institute of High Performance Computing of the Agency for Science, Technology and Research (A*STAR) in Singapore. The DFT calculations were performed at the A*STAR Computational Resource Center (A*CRC).

■ REFERENCES

(1) Fujishima, A.; Honda, K. *Nature* **1972**, *238*, 37–38.
(2) Khan, S. U. M.; Al-Shahry, M.; Ingler, W. B., Jr. *Science* **2002**, *297*, 2243–2245.
(3) Zhu, W.; Qiu, X. F.; Iancu, V.; Chen, X.-Q.; Pan., H.; Wang., W.; Dimitrijevic, N. M.; Rajh, T.; Meyer, H. M.; Paranthaman, M. P.; Stocks, G. M.; Weitering, H. H.; Gu, B. H.; Eres, G.; Zhang, Z. Y. *Phys. Rev. Lett.* **2009**, *103*, 226401.
(4) Asahi, A.; Morikawa, T.; Ohwaki, T.; Aoki, K.; Taga, Y. *Science* **2001**, *293*, 269–271.
(5) Borgarello, E.; Kiwi, J.; Gratzel, M.; Pelizzetti, E.; Visca, M. *J. Am. Chem. Soc.* **1982**, *104*, 2996–3002.
(6) In, S.; Orlov, A.; Berg, R.; Garcia, F.; Pedrosa-Jimenez, S.; Tikhov, M. S.; Wright, D. S.; Lambert, R. M. *J. Am. Chem. Soc.* **2007**, *129*, 13790–13791.
(7) Pan, H.; Guo., B.; Zhang., Z. *J. Chem. Theory Comput.* **2009**, *5*, 3074–3078.
(8) Wendt, S.; Sprunger, P. T.; Lira, E.; Madsen, G. K. H.; Li, Z.; Hansen, J. Ø.; Matthiesen, J.; Blekinge-Rasmussen, A.; Lægsgaars, E.; Hammer, B.; Besenbacger, F. *Science* **2008**, *320*, 1755–1759.
(9) Chen, X.; Mao, S. S. *Chem. Rev.* **2007**, *107*, 2891–2959.
(10) Gratzel, M. *Nature* **2001**, *414*, 338–344.
(11) Bak, T.; Nowotny, W. K.; Sheppard, L. R.; Nowotny, J. *J. Phys. Chem. C* **2008**, *112*, 12981–12987.
(12) Linsebigler, A. L.; Lu, G.; Yates, J. T. *Chem. Rev.* **1995**, *95*, 735–758.
(13) Osterloh, F. E. *Chem. Mater.* **2008**, *20*, 35–54.
(14) Yashima, M.; Teramura, K.; Lu, D. L.; Takata, T.; Saito, N.; Inoue, Y.; Domen, K. *Nature* **2006**, *440*, 295.
(15) Jensen, L. L.; Muckerman, J. T.; Newton, M. D. *J. Phys. Chem. C* **2008**, *112*, 3439–3446.
(16) Wang, X.; Maeda, K.; Thomas, A.; Takanabe, K.; Xin, G.; Carlsson, J. M.; Domen, K.; Antonietti, M. *Nat. Mater.* **2009**, *8*, 76–80.
(17) Hohenberg, P.; Kohn, W. *Phys. Rev.* **1964**, *136*, B864–B871.
(18) Perdew, J. P.; Y. Wang, Y. *Phys. Rev. B* **1992**, *45*, 13244–13249.
(19) Kresse, G.; Furthmüller, J. *Phys. Rev. B* **1996**, *54*, 11169–11186.
(20) Monkhorst, H. J.; Pack, J. D. *Phys. Rev. B* **1976**, *23*, 5188–5192.
(21) Kroke, E.; Schwarz, M. *Coord. Chem. Rev.* **2004**, *248*, 493–532.
(22) Zhang, S. B. *J. Phys.: Condens. Matter* **2002**, *14*, R881–R903.
(23) Pan, H.; Feng, Y.; Lin, J. *Phys. Rev. B* **2006**, *73*, 0345420.
(24) Gracia, J.; Kroll, P. *J. Mater. Chem.* **2009**, *19*, 3020–3026.
(25) Hamada, H.; Sawada, S.; Oshiyama, A. *Phys. Rev. Lett.* **1992**, *68*, 1579–1581.
(26) Pan, H.; Feng, Y.; Lin, J. *Phys. Rev. B* **2006**, *74*, 045409.
(27) Richard, C.; Balavoine, F.; Schultz, P.; Ebbesen, T. W.; Mioskowski, C. *Science* **2003**, *300*, 775–778.
(28) Tang, X. P.; Kleinhammes, A.; Shimoda, H.; Fleming, L.; Bennoune, K. Y.; Sinha, S.; Bower, C.; Zhou, O.; Wu, Y. *Science* **2000**, *288*, 492–494.
(29) Pan, H.; Feng, Y.; Lin, J. *Phys. Rev. B* **2004**, *70*, 245425.
(30) Meng, S.; Kaxiras, E.; Zhang, Z. Y. *Nano Lett.* **2007**, *7*, 663–667.